Rab18 and a Rab18 GEF complex are required for normal ER structure

Andreas Gerondopoulos,[1] Ricardo Nunes Bastos,[1] Shin-ichiro Yoshimura,[2] Rachel Anderson,[1] Sarah Carpanini,[3] Irene Aligianis,[4] Mark T. Handley,[4] and Francis A. Barr[1]

[1]Department of Biochemistry, University of Oxford, Oxford OX1 3QU, England, UK
[2]Department of Cell Biology, Graduate School of Medicine, Osaka University, Suita, Osaka 565-0871, Japan
[3]Division of Neurobiology, The Roslin Institute and Royal (Dick) School of Veterinary Studies, University of Edinburgh, Edinburgh EH25 9RG, Scotland, UK
[4]MRC Human Genetics Unit, Institute of Genetics and Molecular Medicine, University of Edinburgh, Edinburgh EH4 2XU, Scotland, UK

The ancestral Rab GTPase Rab18 and both subunits of the Rab3GAP complex are mutated in the human neurological and developmental disorder Warburg Micro syndrome. Here, we demonstrate that the Rab3GAP complex is a specific Rab18 guanine nucleotide exchange factor (GEF). The Rab3GAP complex localizes to the endoplasmic reticulum (ER) and is necessary for ER targeting of Rab18. It is also sufficient to promote membrane recruitment of Rab18. Disease-associated point mutations of conserved residues in either the Rab3GAP1 (T18P and E24V) or Rab3GAP2 (R426C) subunits result in loss of the Rab18 GEF and membrane-targeting activities. Supporting the view that Rab18 activity is important for ER structure, in the absence of either Rab3GAP subunit or Rab18 function, ER tubular networks marked by reticulon 4 were disrupted, and ER sheets defined by CLIMP-63 spread out into the cell periphery. Micro syndrome is therefore a disease characterized by direct loss of Rab18 function or loss of Rab18 activation at the ER by its GEF Rab3GAP.

Introduction

Rab18 is one of the most highly conserved Rab GTPase regulators of membrane traffic being present in the last eukaryotic common ancestor of both the plant and animal kingdoms (Elias et al., 2012; Klöpper et al., 2012). A defined biological function has remained elusive, partly because it was lost in the budding yeast lineage used for the genetic screens for regulators of membrane traffic. Rab18 has been linked to lipid droplet formation (Martin et al., 2005; Ozeki et al., 2005), ER–Golgi trafficking (Dejgaard et al., 2008), and the regulation of secretory granules (Vazquez-Martinez et al., 2007) and peroxisomes (Gronemeyer et al., 2013), and may be exploited during hepatitis C infection (Salloum et al., 2013). However, no clear molecular function or site of action has been defined for Rab18, despite the fact that loss-of-function mutations are found in the autosomal-recessive human neurological and developmental disorder Warburg Micro syndrome (Bem et al., 2011). These children suffer from multiple specific developmental abnormalities in brain and eye development, profound global developmental delay, and neurodegeneration (Bem et al., 2011). However, the pattern of Rab18 conservation in both plants and animals indicates that the essential cellular function is unlikely to be specific to neuronal cells (Lütcke et al., 1994; Klöpper et al., 2012).

In addition to Rab18, a known Rab regulatory complex is mutated in Warburg Micro syndrome (Aligianis et al., 2005, 2006; Handley and Aligianis, 2012; Handley et al., 2013). This is the Rab3 GTPase-activating protein (GAP) complex originally identified using biochemical purification from brain tissue as a cellular factor promoting GTP hydrolysis by Rab3 (Fukui et al., 1997; Nagano et al., 1998). Like Rab18, the Rab3GAP complex is both more widely conserved and more broadly expressed than Rab3 and is ubiquitously expressed in human tissues (Nagano et al., 1998), raising the possibility that regulation of Rab3 is not its only function.

Simple logic suggests that the Rab3GAP complex and Rab18 act in the same pathway because mutations result in the same disease phenotype. We therefore set out to identify the cellular site of action of Rab18 and its functional relationship with Rab3GAP. Two simple alternatives present themselves, either

Correspondence to Francis A. Barr: francis.barr@bioch.ox.ac.uk; or Mark T. Handley: mark.handley@igmm.ed.ac.uk

Abbreviations used in this paper: GAP, GTPase-activating protein; GEF, guanine nucleotide exchange factor; Rtn4, reticulon 4.

The Rockefeller University Press $30.00
J. Cell Biol. Vol. 205 No. 5 707–720
www.jcb.org/cgi/doi/10.1083/jcb.201403026

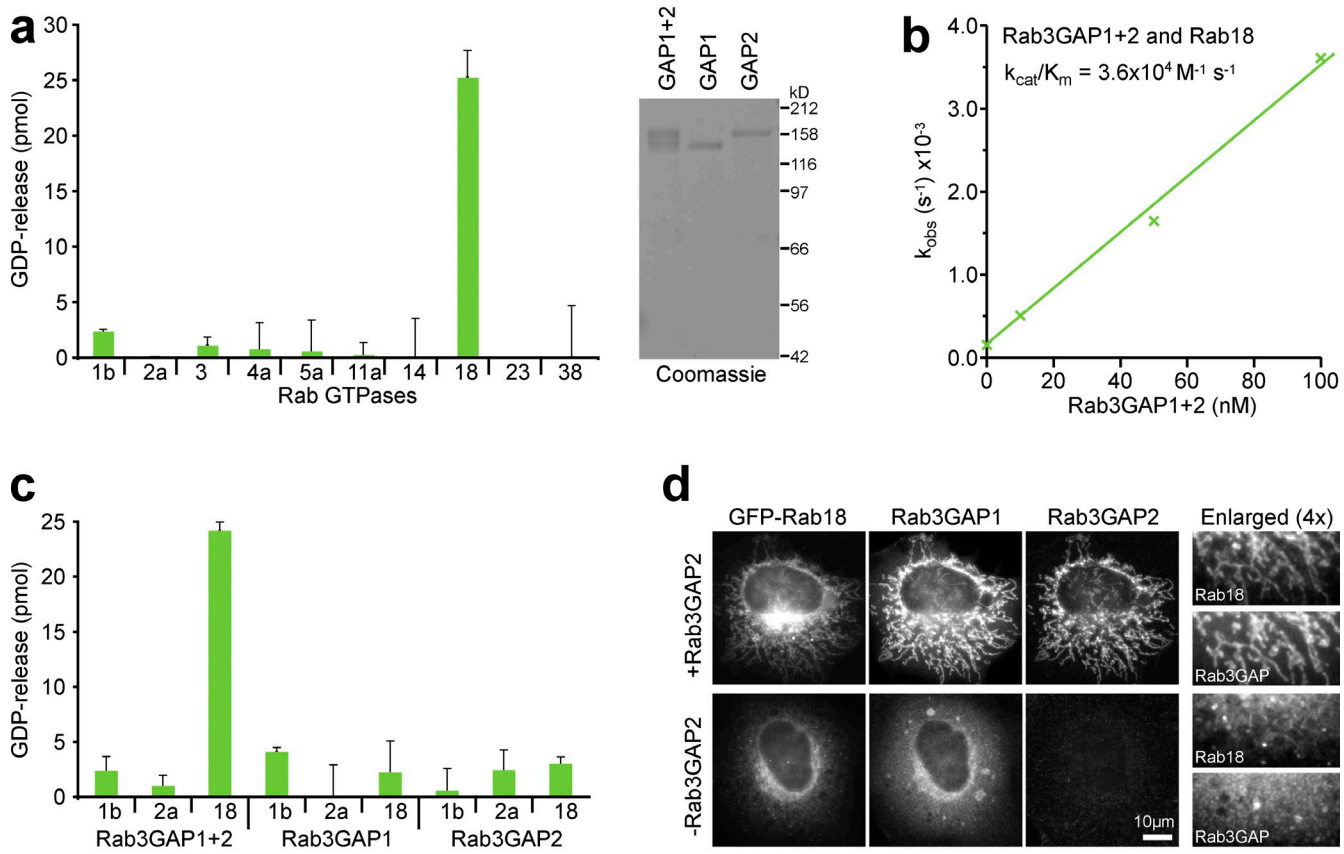

Figure 1. **Rab3GAP is a Rab18 GEF.** (a) Rab3GAP complexes were used for GEF assays toward a representative group of Rab GTPases. Error bars indicate the standard deviation of the mean (n = 3). Rab3GAP complexes and individual subunits (GAP1 and GAP2) were analyzed on protein gels stained with colloidal Coomassie brilliant blue stain. (b) Mant-GDP kinetic GEF assays were performed using the Rab3GAP complex and Rab18 as a substrate to derive catalytic efficiency (k_{cat}/K_m). Initial rates of nucleotide exchange were derived from three independent experiments and are plotted as a function of Rab3GAP concentration. (c) Rab3GAP complexes and individual subunits were used for GEF assays toward Rab1b, Rab2a, and Rab18. Error bars indicate the standard deviation of the mean (n = 3). (d) HeLa cells were cotransfected for 20 h with GFP-Rabs and Myc-tagged Rab3GAP1 in the presence and absence of the Tom70-FLAG-Rab3GAP2 mitochondrial-targeting fusion. The cells were fixed and then stained with FLAG and Myc antibodies; Rabs were visualized using GFP fluorescence. Bars are marked in the figure.

Rab3GAP acts downstream of Rab18 as an effector complex for the active GTP form of Rab18, or Rab3GAP acts upstream of Rab18 as a potential guanine nucleotide exchange factor (GEF) regulator promoting Rab18 activation. The evidence presented here provides strong support for the hypothesis that the Rab3GAP complex is the cellular GEF activating Rab18, and this activity is required for Rab18 localization to the ER where it acts in a pathway maintaining normal ER morphology.

Results

Rab3GAP is a Rab18 GEF

Most disease-causing mutations in Rab3GAP1 are frameshift and nonsense mutations likely to affect protein expression (Handley and Aligianis, 2012; Handley et al., 2013). However, several missense loss-of-function mutations cluster in a highly conserved N-terminal domain of Rab3GAP1, suggesting this is an important function determinant of Rab3GAP activity discrete from the C-terminal Rab3 GAP domain (Handley and Aligianis, 2012; Handley et al., 2013). Rab3GAP is a binary complex formed from two different subunits and mutations in either subunit cause Micro syndrome (Handley and Aligianis, 2012; Handley et al., 2013). Thus, if Rab3GAP functions as a Rab GEF, both of its subunits could be required for full nucleotide exchange activity. We therefore tested the in vitro nucleotide exchange activity of a purified Rab3GAP complex in addition to that of the individual Rab3GAP1/2 subunits (Fig. 1 a, see inset showing Coomassie brilliant blue–stained gel). Screening against a panel of Rabs revealed a specific GDP release activity directed toward Rab18, whereas no activity was seen toward Rab3, the other Rab implicated in Micro syndrome (Fig. 1 a). Kinetic analysis showed that catalytic efficiency (k_{cat}/K_m) toward Rab18 is 3.6×10^4 $M^{-1}s^{-1}$ (Fig. 1 b). By comparison, the catalytic efficiencies of Rabex5 and DENND1 GEFs for Rab5 and Rab35 are $\sim 2.5 \times 10^4$ $M^{-1}s^{-1}$ (Delprato et al., 2004; Delprato and Lambright, 2007; Wu et al., 2011). Both subunits were required for this Rab18 GEF activity, and neither subunit alone stimulated GDP release above the basal level seen with other nontarget Rabs (Fig. 1 c).

Rab GEFs form part of the minimal machinery needed for Rab targeting (Barr, 2013; Blümer et al., 2013). The ability of the Rab3GAP complex to promote Rab18 recruitment to a heterologous membrane in vivo was therefore tested (Gerondopoulos et al., 2012). When Rab3GAP2 was ectopically targeted to mitochondria,

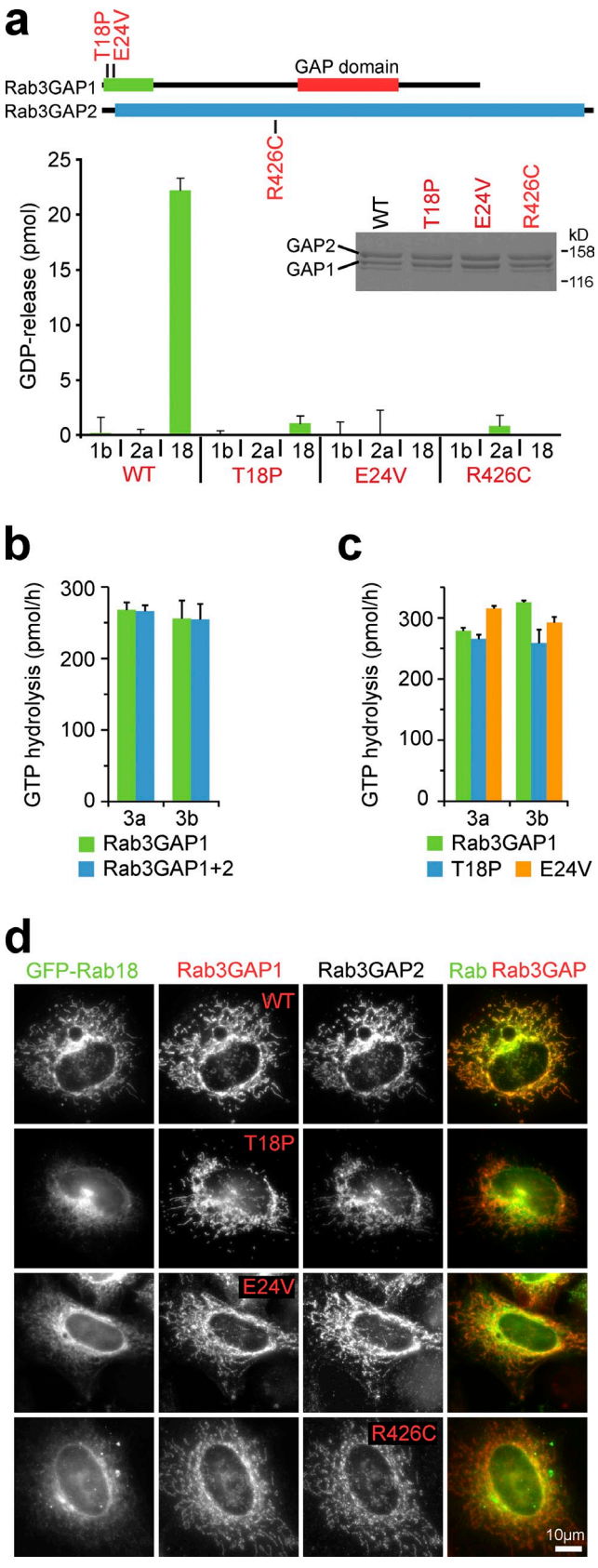

Figure 2. **Disease-associated mutations in Rab3GAP1 and Rab3GAP2 result in loss of Rab18 GEF activity.** (a) A schematic of the Rab3GAP complex showing the Rab3 GAP domain and the conserved N-terminal region of Rab3GAP1. Pathological missense mutations in Rab3GAP1 and Rab3GAP2 are marked. Wild-type and disease mutant Rab3GAP complexes were used for GEF assays toward Rab1b, Rab2a, and Rab18. Error bars indicate the standard deviation of the mean (n = 3). (b) Wild-type Rab3GAP1, Rab3GAP1 and Rab3GAP2, or (c) wild-type and disease mutant Rab3GAP1 were used for GTPase assays with Rab3a or Rab3b. Error bars indicate the range (n = 2). This is a subset of the full screening data presented in the inset bar graph panel of Fig. S1 a. (d) HeLa cells were cotransfected for 20 h with GFP-Rabs, wild-type and disease mutant Myc-tagged Rab3GAP1, and the Tom70-FLAG-Rab3GAP2 mitochondrial-targeting fusion as indicated in the figure. The cells were fixed and then stained with FLAG and Myc antibodies; Rabs were visualized using GFP fluorescence. Bars are marked in the figure.

its expression triggered recruitment of both coexpressed Rab3GAP1 and Rab18 to this compartment (Fig. 1 d). Omission of Rab3GAP2 resulted in loss of this Rab18 recruitment activity (Fig. 1 d). Rab3GAP therefore fulfils the requirements expected of a specific and highly active Rab18 GEF by promoting membrane association of Rab18.

Effect of disease-associated mutations on Rab18 GEF activity

The effects of known disease-causing point mutations in Rab3GAP1 and Rab3GAP2 were then tested. First, recombinant Rab3GAP complexes were made using Rab3GAP1 T18P or E24V and wild-type Rab3GAP2, or wild-type Rab3GAP1 and Rab3GAP2 R426C (Fig. 2 a). Of these complexes, only the form with both wild-type subunits showed activity toward Rab18 (Fig. 2 a). Complexes carrying either a mutant Rab3GAP1 or Rab3GAP2 subunit showed no activity toward Rab18 above the basal level seen with related nontarget Rabs (Fig. 2 a). Analysis of the GAP activity of the complex toward Rab3a and Rab3b showed that this is due to the Rab3GAP1 subunit of the complex and does not require the Rab3GAP2 subunit (Fig. 2 b). Furthermore, screening of Rab3GAP1 against a panel of human Rabs confirmed that it showed greatest activity toward Rab3a, Rab3b, and Rab3c, as expected (Fukui et al., 1997; Nagano et al., 1998), but also has some activity toward a subset of other Rabs, although not Rab18 (Fig. S1 a). However, disease-associated point mutants in Rab3GAP1 had no effect on the GAP activity toward the Rab3 family, or the other potential targets Rab5a and Rab43 (Fig. 2 c; and Fig. S1 a, inset bar graph). No GAP activity of either wild-type or mutant Rab3GAP1 toward Rab18 was detected.

In agreement with the biochemical data defining a specific Rab18 GEF activity, the ability of the resulting mutant complexes to drive mitochondrial recruitment of Rab18 was abolished in the heterologous membrane-targeting assay (Fig. 2 d). These same mutations did not affect the capacity of Rab3GAP2 to recruit Rab3GAP1. The Rab3GAP complex is therefore a Rab18 GEF that forms part of the membrane-targeting machinery for Rab18, and Rab3GAP mutations associated with Micro syndrome disrupt this activity. These same mutations do not alter the GAP activity of this complex toward Rab3, making it unlikely that reduced GTP hydrolysis by Rab3 is the major change leading to Warburg Micro syndrome.

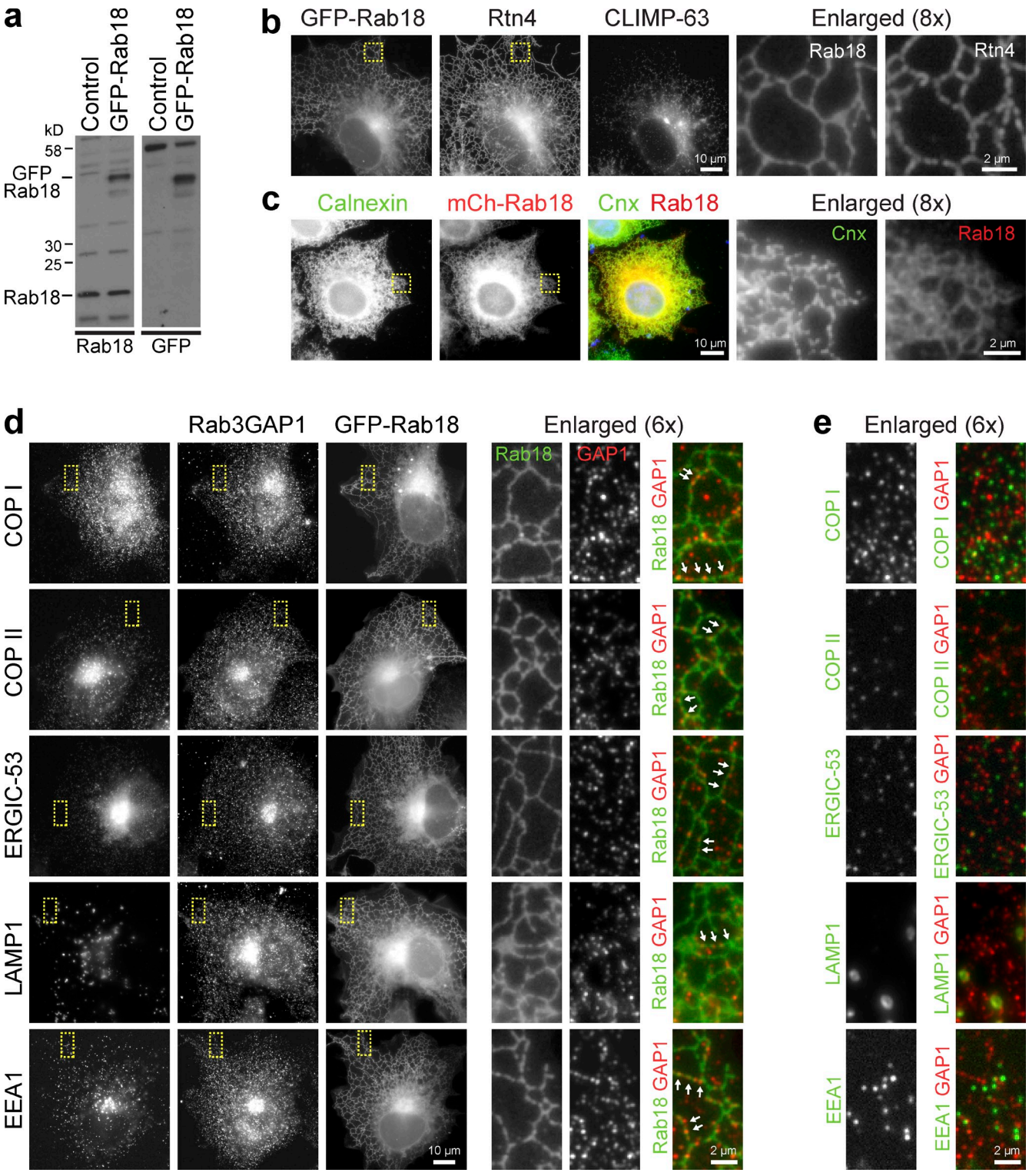

Figure 3. **Analysis of Rab18 and Rab3GAP localization to the ER.** (a) Western blot of COS7 control cells and COS7 cells expressing GFP-Rab18 with antibodies to endogenous Rab18 and GFP. (b) GFP-Rab18, reticulon 4 (Rtn4), and CLIMP-63 staining is shown in COS7 cells. (c) Calnexin staining and mCherry (mCh)-tagged Rab18 are shown in HeLa cells. (d) COS7 cells expressing GFP-Rab18 were stained for Rab3GAP1 and markers for COP I (β-COP), COP II (Sec31), ERGIC-53, and LAMP1. Arrowheads in the enlarged region show details of Rab3GAP1 localization to ER tubules marked by GFP-Rab18. (e) The enlarged region corresponding to the yellow boxed area in d shows details of the Rab3GAP1 and different compartment markers. Bars are marked in the figure.

Localization of Rab18 and Rab3GAP to the ER

Because of differing reports that Rab18 is present on lipid droplets, Golgi, and other organelles of the secretory pathway, the localization of Rab18 was investigated. Because antibodies capable of specifically detecting Rab18 on Western blots (Fig. S1 b) failed to detect any specific signal in immunofluorescence using a variety of different fixation protocols, cells expressing GFP-Rab18 were used. Western blotting showed that GFP-Rab18 was expressed at a similar level to the endogenous protein in COS7 cells (Fig. 3 a). These cells were then stained with the ER tubule and sheet markers reticulon 4 (Rtn4) and CLIMP-63, respectively. At this level of expression, Rab18 was present on ER tubules marked by Rtn4 (Fig. 3 b), a region lacking the ER sheet marker CLIMP-63. In HeLa cells, mCherry-tagged Rab18 was found to be present in both the perinuclear region and the cell periphery and to overlap with the ER marker calnexin (Fig. 3 c).

The localization of the Rab3GAP complex was then investigated using an antibody to the Rab3GAP1 subunit. Rab3GAP1 was detected in punctate structures spread throughout the volume of the cell (Fig. 3 d). Many of these punctate structures overlapped with Rab18-positive ER tubules in the cell periphery (Fig. 3 d, marked by arrows in the enlarged region). However, they did not show any overlap with markers for either COP I or COP II vesicles, the ER–Golgi recycling compartment marker ERGIC-53, or the endosome and lysosome markers EEA1 and LAMP1 (Fig. 3 d, and the enlarged region in Fig. 3 e). These observations are consistent with the idea that the Rab3GAP complex could activate Rab18 at the ER. However, the pattern of localization suggests that the Rab3GAP complex is restricted to a subdomain of the ER.

Rab3GAP complex regulates ER localization of Rab18

The requirement for Rab3GAP in Rab18 localization to the ER was then tested. Western blotting confirmed that Rab3GAP subunits, Rab18, and the negative control Rab7 were all efficiently depleted (Fig. S1 b). Furthermore, depletion of either subunit by siRNA affects levels of the other (Fig. S1 b), consistent with a report that deletion of Rab3GAP1 in mice results in loss of Rab3GAP2 protein (Sakane et al., 2006). Depletion of either subunit of the Rab3GAP complex resulted in loss of Rab18 from ER tubules and accumulation in a diffuse pattern most probably reflecting cytoplasmic localization in over 80% of cells (Fig. 4, a and b). Biochemical fractionation showed that in control cells Rab18 was found only in the membrane fraction, and in the absence of the Rab3GAP complex it was partially redistributed to the cytosol fraction (Fig. 4 c).

The role of Rab18 activation in the dynamics of the ER was then followed using live-cell imaging of mCherry-tagged Rab18 and a GFP-tagged ER marker. Dynamic tubular networks undergoing rapid branch migration and the formation of new connections by tubule fusion characterized the ER in control cells (Fig. 4 d and Video 1), as expected. These features were lost in the absence of the Rab18 GEF. Depletion of either Rab3GAP1 or Rab3GAP2 alone or in combination resulted in the loss of Rab18 from defined ER tubules and redistribution to a diffuse cytoplasmic pattern (Fig. 4 d). In addition to the loss of Rab18-positive tubular networks, ER sheets with dynamic edges extended into the cell periphery (Fig. 4 d and Videos 2–5). These results support the idea that Rab18 membrane association and localization to the ER requires the activity of its cognate GEF in the form of the Rab3GAP complex. They also suggest that the Rab18 pathway is important for maintaining the structure of the ER.

Altered ER morphology in the absence of Rab18 or the Rab3GAP complex

The ER can be divided into a perinuclear region defined by the marker CLIMP-63, whereas the peripheral ER tubular network lacks CLIMP-63 but is positive for Rtn4 (Voeltz and Prinz, 2007; Friedman and Voeltz, 2011). A role for Rab3GAP and Rab18 function in supporting this organization was tested in two different cell lines. When COS7 cells were depleted of Rab3GAP subunits or Rab18, CLIMP-63 spread away from the perinuclear region into the cell periphery, suggesting that ER sheets are expanded under these conditions (Fig. 5 a). This spread in CLIMP-63 was highly penetrant and observed in ∼80% of cells depleted of Rab3GAP subunits or Rab18 (Fig. 5 b, green bars). Measurements of the area occupied by CLIMP-63 indicated that ER sheet volumes increased from 30% of the cell area to 60–80% in cells depleted of Rab3GAP subunits or Rab18 (Fig. 5 b, blue bars). In addition to the redistribution of Rab18 from the ER to the cytoplasm, HeLa cells depleted of Rab3GAP also showed a loss of calnexin staining in peripheral ER tubular networks (Fig. S1 c). Quantitation again confirmed that this was a highly penetrant effect, and fewer than 20% of Rab18- or Rab3GAP complex–depleted cells showed calnexin in peripheral ER tubular networks, compared with greater than 90% of control cells (Fig. S1, d and e). No alterations in the ER–Golgi Sec31 COP II vesicle coat protein or TGN46 trans-Golgi markers were observed in HeLa cells (Fig. S2 a). Similarly, the ERGIC-53 ER–Golgi recycling compartment marker and the TGN46 trans-Golgi marker were not obviously altered when Rab18 or the Rab3GAP complex was depleted in COS7 cells (Fig. S2 b). Western blots did not reveal major changes in the ER chaperones BIP, ERp72, or calnexin (Fig. S3 a), suggesting that the observed changes in ER morphology are not the result of a stress response and instead reflect a specific function for Rab18 at the ER.

To eliminate the possibility that indirect or off-target effects of the RNA interference procedure caused altered ER structure, rescue experiments were performed for Rab18. Cells were treated with two different Rab18 siRNA duplexes directed to the 3′UTR of the mRNA, then transfected with empty vector or GFP-tagged Rab18. Depletion of Rab18 using the Rab18.8 3′UTR duplex resulted in the spread of CLIMP-63 into the peripheral region, and this was reversed by expression of GFP-Rab18 resistant to the siRNA (Fig. 6 a). Western blotting showed that the level of GFP-Rab18 was similar to that of the endogenous Rab18, and that depletion of Rab18 was efficient under these conditions (Fig. 6 b). Measurements of the area occupied by CLIMP-63 indicated that ER sheet volumes increased from 30% of the cell area to 60–80% in cells depleted of Rab18 with either of the Rab18 3′UTR

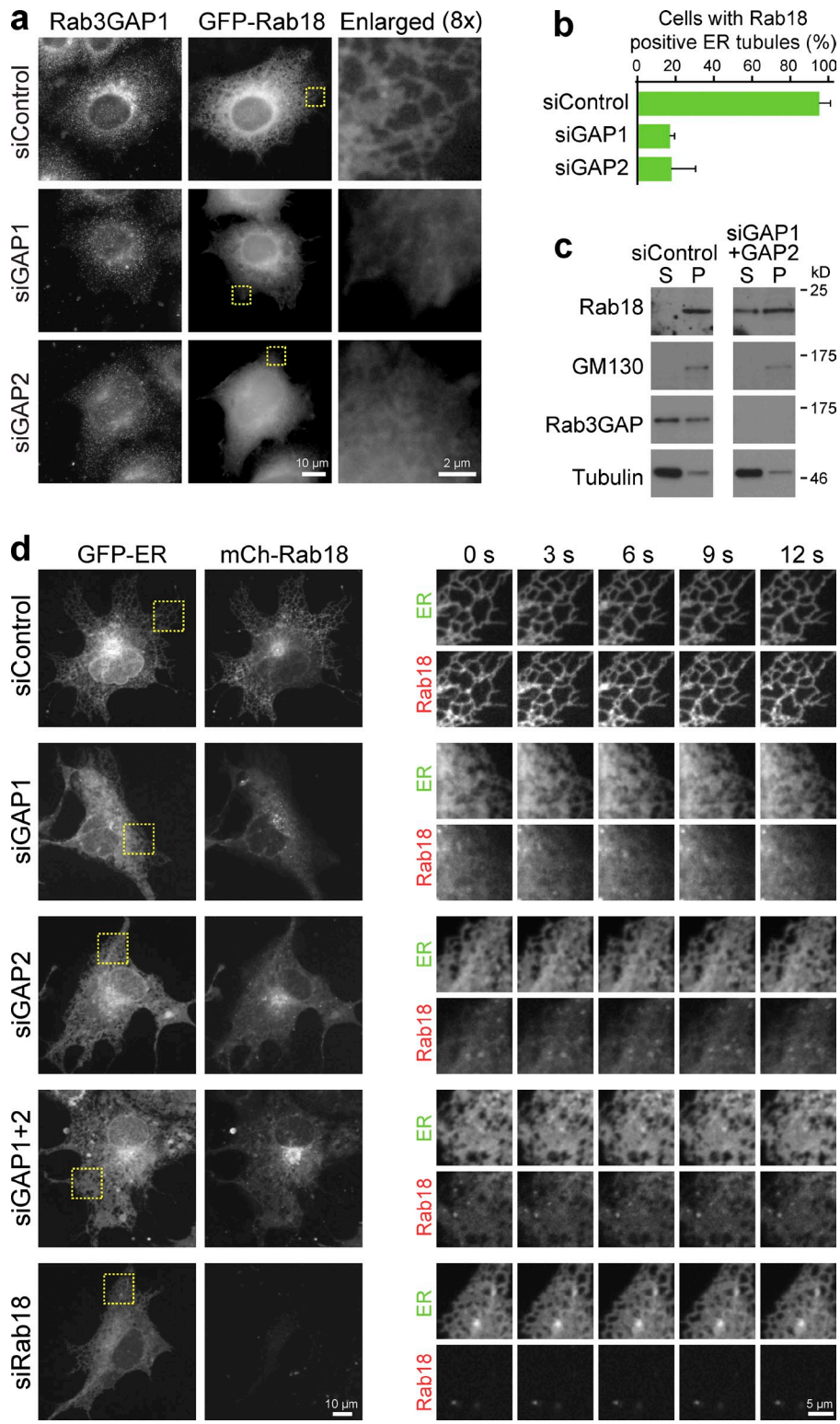

Figure 4. **Rab3GAP is required for ER localization of Rab18.** (a) HeLa cells expressing GFP-Rab18 were depleted of Rab3GAP subunits (siGAP1 and siGAP2) for 72 h and then stained with a Rab3GAP1 antibody. The enlarged region from the yellow boxed area shows details of Rab18 localization. (b) The presence of GFP-Rab18 on ER tubules was scored for all conditions and plotted in the bar graph. Error bars indicate the standard deviation of the mean (n = 3 independent experiments). (c) HeLa cells were depleted of Rab3GAP subunits (GAP1 and GAP2) for 72 h. Western blots show the distribution of endogenous Rab18 to the membrane pellet (P) and soluble (S) cytosol fractions marked by the Golgi membrane protein GM130 and tubulin, respectively. Rab3GAP1 depletion was confirmed by Western blotting. (d) COS7 cells expressing a GFP-tagged ER marker and mCherry-tagged Rab18 were depleted of Rab3GAP subunits alone or in combination or Rab18 for 72 h then imaged at 1.5-s intervals using a spinning-disk confocal microscope. The entire cell is shown for t = 0, and a time series from the yellow boxed area is depicted in the enlarged regions. Bars are marked in the figure.

duplexes tested (Fig. 6 c, green bars). In both cases this effect was rescued by expression of GFP-Rab18 (Fig. 6 c, blue bars). Live-cell imaging of cells depleted of endogenous Rab18 using the Rab18.7 3′UTR duplex resulted in the loss of dynamic ER tubular networks and the expansion of less dynamic sheet areas, and this was reversed by expression of mCherry-Rab18 resistant to the siRNA (Fig. 6 d and Videos 6–8).

Rab10 has previously been implicated in the regulation of ER structure (English and Voeltz, 2013), and its relationship to Rab18 was therefore investigated. Rab10 was depleted efficiently (Fig. S3 a), but this resulted in only a partial spread of ER sheets to the cell periphery (Fig. 5, a and b). The localization of Rab10 and Rab18 was then compared in HeLa and COS7 cells. Whereas Rab18 targeted to ER tubular networks in both

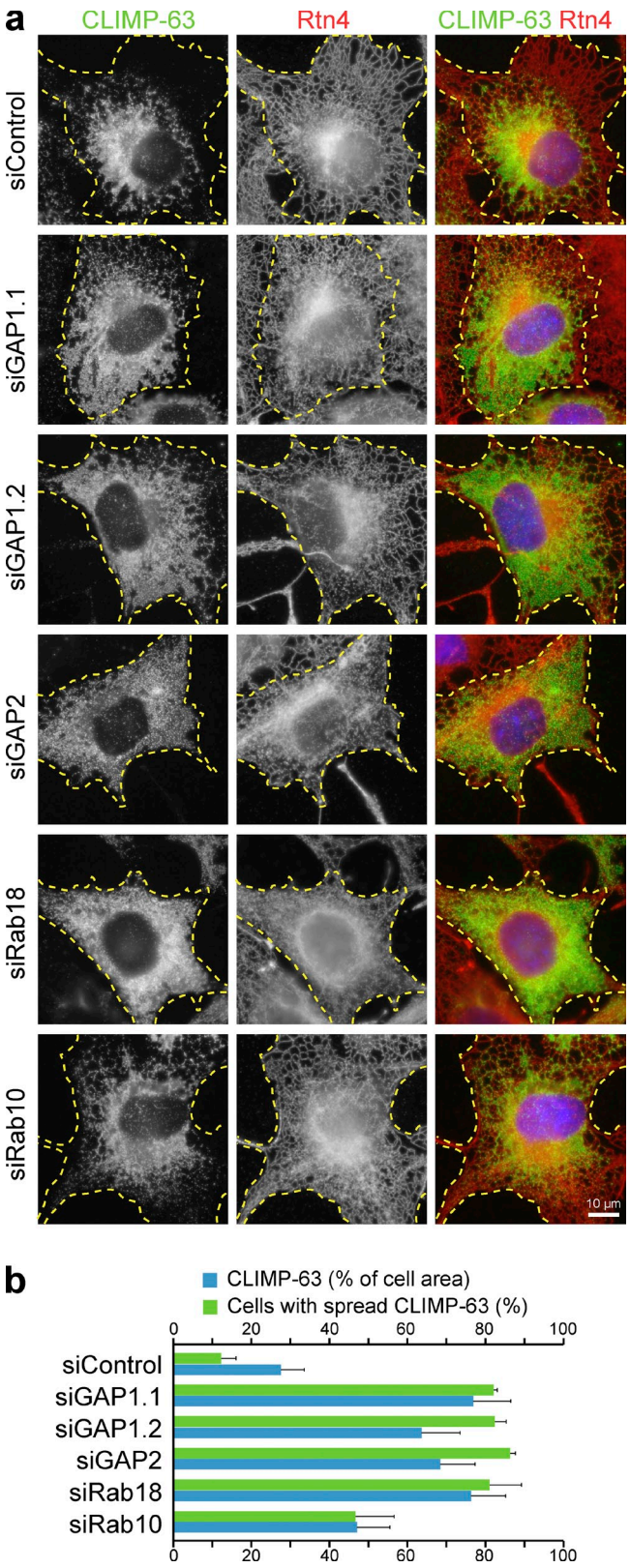

Figure 5. **ER sheets spread into the cell periphery when Rab18 or its GEF complex is depleted.** (a) COS7 cells were depleted of Rab3GAP subunits (GAP1 and GAP2), Rab18, or Rab10 for 72 h. Two different siRNA duplexes to Rab3GAP1 (GAP1.1 and GAP1.2) were used. The cells were fixed and then stained with antibodies to CLIMP-63 and reticulon 4 (Rtn4). DNA was stained with DAPI (blue in the merged panel). Dotted yellow lines mark the cell boundaries. The bar is marked in the figure. (b) The area of CLIMP-63 as a function of total cell area was measured using ImageJ (National Institutes of Health) for 50–70 cells per experiment, for three independent experiments (blue bars). Additionally, the percentage of cells showing spread CLIMP-63 was also counted (green bars). In both cases the mean values are plotted in the bar graph, with error bars indicating the standard deviation of the mean.

cell lines, Rab10 only showed pronounced ER tubule localization in COS7 cells (Fig. S3, b and c). Intriguingly, although depletion of Rab10 did not cause a loss of Rab18 from the ER membrane, it did result in a shift to a partly sheet-like distribution more like that of CLIMP-63 (Fig. S3 d). Although these results support the view that both Rab18 and Rab10 can be detected on the ER, they suggest that these two Rabs have different functions.

Warburg Micro syndrome and ER shaping

To confirm that the ER defects observed in cell lines depleted of Rab18 and Rab3GAP complex subunits are relevant for the human disease, the localization of CLIMP-63 and Rtn4 was investigated in two patient cell lines. These cell lines carried either the Rab18 L24Q nucleotide-binding site mutation, or the Rab3GAP1 (c.649-2A>G) splicing mutation (Aligianis et al., 2005; Bem et al., 2011). In comparison to control fibroblasts, CLIMP-63 spread away from the perinuclear region into the cell periphery and clearly defined Rtn4-positive tubules were lost in both the Rab18 L24Q and Rab3GAP1 (c.649-2A>G) patient cell lines (Fig. 7 a). Measurements of the area occupied by CLIMP-63 indicated that ER sheet volumes increased from 20% of the cell area to 60–70% in cells with mutant Rab18 or Rab3GAP1 (Fig. 7 b). Spread of ER sheets and a loss of fragmentation of ER tubules were therefore observed in patient fibroblasts.

After the initial discovery of Rab3GAP and Rab18 mutations it was found that the ER transmembrane protein TBC1D20 is mutated in Warburg Micro syndrome and the blind sterile mouse (Liegel et al., 2013). TBC1D20 is a GAP for Rab1 and Rab2 with some limited activity toward Rab18 in vitro (Haas et al., 2007). TBC1D20 interacts with the reticulon family of ER-shaping proteins (Haas et al., 2007), and has been implicated in secretion (Wendler et al., 2010). The relationship between Rab3GAP complex and TBC1D20 in ER shaping was therefore investigated. As already shown, depletion of the Rab3GAP1 and Rab3GAP2 subunits resulted in the redistribution of Rab18 to the cytoplasm, the spread of the ER sheet marker CLIMP-63, and fragmentation of the peripheral ER tubular network defined by Rtn4 (Fig. 7 c). By contrast, depletion of TBC1D20 resulted in a slight spread of the ER sheets marked by CLIMP-63 (Fig. 7 c). In addition, alterations in the distribution of Rab18 to the peripheral ER reticular network were observed. Instead of precisely following the Rtn4-positive ER tubules as in the control samples, Rab18 spread across the fenestrations in the reticular network (Fig. 7 c). This created a hybrid webbed network in which fingers of Rtn4 are linked by sheets containing Rab18. Therefore, although loss of TBC1D20 function results in altered ER structure, the differences in the phenotype suggest it plays a different role to the Rab3GAP complex and Rab18.

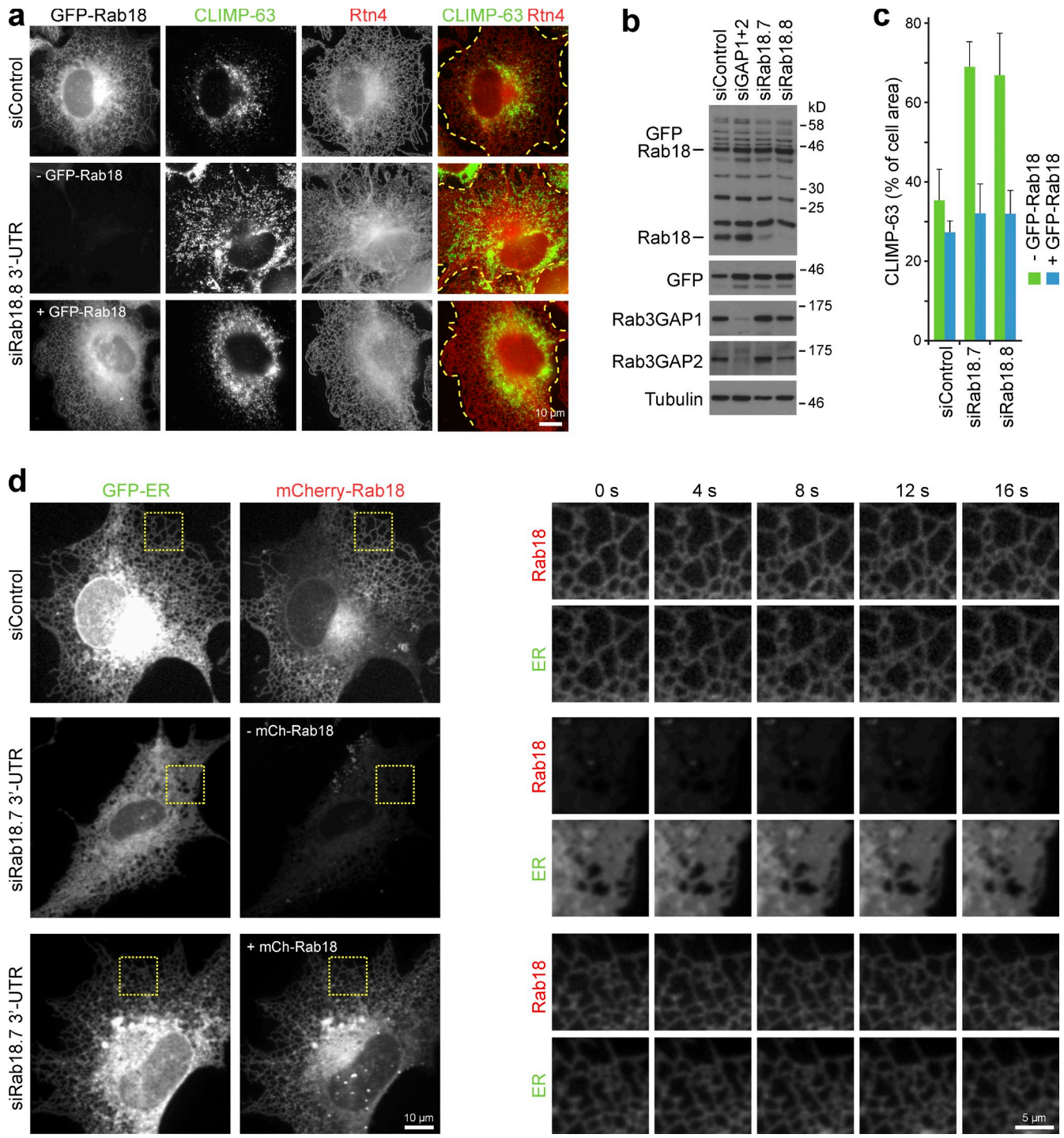

Figure 6. **Loss of dynamic ER tubules in Rab18-depleted cells.** (a) COS7 cells were treated with control or Rab18.8 3′-UTR siRNA for 52 h, then transfected with empty vector or GFP-Rab18 for 20 h. Cells were fixed and then stained with antibodies to CLIMP-63 and Rtn4. Dotted yellow lines mark the cell boundaries. (b) COS7 cells were treated with control, Rab3GAP (siGAP1+2), Rab18.7, or Rab18.8 3′-UTR siRNA for 52 h, then transfected with empty vector or GFP-Rab18 for 20 h. Cell lysates were Western blotted with antibodies to Rab18, GFP, Rab3GAP subunits, and tubulin as a loading control. Rab18 antibodies see multiple nonspecific bands; lines in the figure indicate endogenous Rab18 and GFP-Rab18. (c) The area of CLIMP-63 as a function of total cell area was measured using ImageJ for 40–60 cells per experiment, for three independent experiments. This was performed for cells expressing (blue bars) or not expressing (green bars) GFP-Rab18. Mean values are plotted in the bar graph, with error bars indicating the standard deviation of the mean. (d) COS7 cells expressing a GFP-ER marker were treated with control or Rab18.7 3′-UTR siRNA for 52 h, then transfected with empty vector or mCherry-Rab18 for 20 h. The cells were then imaged at 2-s intervals using a spinning-disk confocal microscope. The entire cell is shown for t = 0, and a time series showing images every 4 s from the yellow boxed area is depicted in the enlarged regions. Bars are marked in the figure.

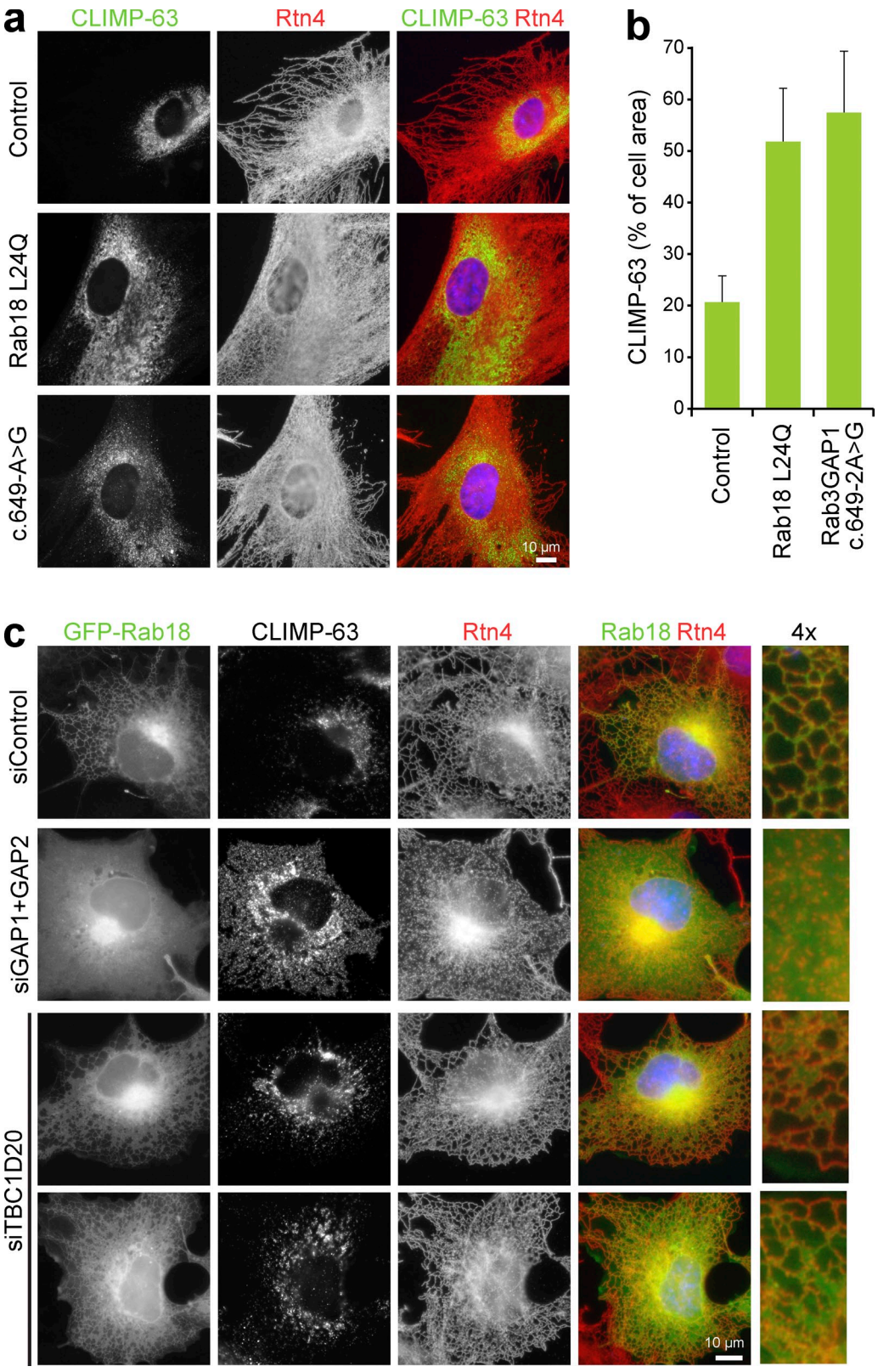

Figure 7. **Warburg Micro syndrome patient cell lines show altered ER morphology.** (a) Control and patient fibroblasts were fixed and then stained with antibodies to CLIMP-63 and reticulon 4 (Rtn4). DNA was stained with DAPI (blue in the merged panel). (b) The area of CLIMP-63 as a function of total cell area was measured using ImageJ for 50–70 cells per experiment, for three independent experiments. The mean values are plotted in the bar graph, with error bars indicating the standard deviation of the mean. (c) COS7 cells expressing GFP-Rab18 were treated with control, Rab3GAP (siGAP1+GAP2), or TBC1D20 siRNA duplexes for 72 h. The cells were fixed and then stained with antibodies to CLIMP-63 and Rtn4. DNA was stained with DAPI (blue in the merged panel). The merged panel shows a comparison of GFP-Rab18 and Rtn4 localization to ER tubular networks. Bars are marked in the figure.

Intriguingly, both TBC1D20 and Rab18 have been linked to ER-associated lipid droplet structures (Martin et al., 2005; Ozeki et al., 2005; Liegel et al., 2013; Salloum et al., 2013). To test if Rab3GAP, Rab18, and TBC1D20 play a general role in lipid droplet formation and turnover, cells were fed oleate–BSA complexes for 18 h to induce lipid droplet formation. These cells were then stained for ER markers CLIMP-63 and Rtn4, and lipid droplets were detected with BODIPY (Fig. S4 a). Western blotting confirmed efficient depletion of target proteins (Fig. S4 b). Compared with the control cells, BODIPY stained larger more intense structures clustered against the nucleus after depletion of Rab18 pathway components or TBC1D20 (Fig. S4 a), suggesting more lipid was stored. A time-course analysis of lipid storage and turnover revealed that after 18 h, cells depleted of Rab3GAP complex subunits, Rab18, or TBC1D20 showed twofold higher staining with BODIPY than control cells (Fig. S4 c). In all cases, after removal of oleate by transfer to fresh growth medium this signal declined at the same rate over the following 36 h (Fig. S4 d). Rab18, Rab3GAP, and TBC1D20 are therefore not essential for lipid droplet formation or turnover under these conditions. Furthermore, neither mCherry-tagged Rab18 nor the ER tubular network marker Rtn4 showed any obvious enrichment on lipid droplet structures (Fig. S5 a). Live-cell imaging showed that lipid droplets often lie adjacent to the ER tubular networks in control cells (Fig. S5 b) and move together with Rab18-positive ER tubular networks (Video 9). However, in cells depleted of Rab18 or the Rab3GAP complex, lipid droplets showed an increased rather than decreased association with ER sheets (Fig. S5 b). This change could potentially facilitate lipid storage without requiring a direct role for Rab18 or the Rab3GAP complex in lipid droplet biogenesis.

Discussion

Rab3GAP is a Rab18 GEF

Rab3GAP1 and Rab3GAP2 were originally isolated from bovine brain as subunits of a complex promoting GTP hydrolysis by Rab3 (Fukui et al., 1997; Nagano et al., 1998). This has led to the suggestion that a defect in neurotransmission resulting from altered Rab3 function contributes to Warburg Micro syndrome (Aligianis et al., 2005, 2006). As we show here, the Rab3GAP complex also has specific and potent Rab18 GEF activity. Supporting the view that Rab18 is the physiological target of Rab3GAP, the catalytic efficiency of $3.6 \times 10^4\ M^{-1}s^{-1}$ is equivalent to Rab GEFs with known targets (Langemeyer et al., 2014). In agreement with this idea, disease-associated mutations in Rab3GAP abolish this Rab18 GEF activity and cause a loss of Rab18 from the ER in fibroblast cell lines. The presence of Rab18 (Elias et al., 2012; Klöpper et al., 2012) and the Rab3GAP complex in a wide variety of eukaryotes lacking Rab3, including plants, also supports the view that the essential cellular function of this pathway is not the regulation of neurotransmission. Neurological dysfunction may therefore be caused by more fundamental cellular defects linked to perturbed ER function.

ER regulation by Rab GTPase pathways

The ER is organized into two morphologically discrete domains, the perinuclear ER sheets and peripheral tubular networks (Voeltz and Prinz, 2007; Friedman and Voeltz, 2011). These domains are further specialized into functional regions, including the so-called ER exit sites where biosynthetic cargo transport occurs, sites where lipid droplets form, and contact sites with other cellular organelles such as mitochondria, endosomes, and the plasma membrane (Friedman and Voeltz, 2011; Rowland and Voeltz, 2012). However, in most cases an essential requirement for normal ER morphology in these processes remains unclear. A series of factors required for ER tubular network formation have been identified, and these can be divided into factors promoting ER tubule formation such as the reticulon, DP1 and REEP integral membrane protein family (Voeltz et al., 2006; Shibata et al., 2008; Park et al., 2010), and transmembrane GTPases of the atlastin family promoting ER tubule fusion to generate networks (Hu et al., 2009; Orso et al., 2009). Less is known about the mechanism of sheet formation, but the transmembrane protein CLIMP-63 is thought to localize to and stabilize ER sheets by acting as a luminal spacer (Klopfenstein et al., 2001; Shibata et al., 2010).

Rab GTPases can now be added to this emerging picture. In contrast to the factors already discussed, which are integral membrane proteins, Rabs are peripheral membrane proteins recruited from the cytosol thought to act as regulators of membrane fusion and organelle identity (Barr, 2013; Pfeffer, 2013). Rab10 is associated with ER networks and promotes ER tubule dynamics (English and Voeltz, 2013). In polarized cells, Rab10 and its cognate GEF DENND4/CRAG are required together with a transmembrane sorting receptor TANGO1 for the basolateral transport of collagen (Yoshimura et al., 2010; Lerner et al., 2013). This raises the intriguing possibility that polarized transport is already specified at the level of the ER. However, how Rab10 is activated at the ER and what its downstream effector proteins are remains unclear.

In this work we show that the Rab3GAP complex activates Rab18, and this is required for Rab18 recruitment to the ER. Further studies will be needed to define the downstream effector pathways coupling to Rab18, and it would be premature to specify what precise events Rab18 regulates. It may directly act in the pathway of lipid droplet biogenesis; however, details of effectors are crucial. The altered ER structure reported here suggests that Rab18 effectors may regulate ER tubule tethering and fusion, or perhaps act as inhibitors of ER sheet extension. Understanding the interplay between Rab18, Rab10, and tubular network–promoting factors of the reticulon and atlastin families will therefore be an important goal for future work.

Previous studies have implicated Rab18 in lipid droplet formation, and have reported that Rab18 is highly enriched on lipid droplets (Martin et al., 2005; Ozeki et al., 2005). However, these studies relied on high-level expression of Rab18 to induce alterations in lipid droplet apposition to ER membranes and Rab18 localization to lipid droplets (Martin et al., 2005; Ozeki et al., 2005). Under the conditions used here, where tagged Rab18 was expressed at levels similar to the endogenous protein, Rab18 was found on tubular networks forming the ER and was not enriched on lipid droplets. Lipid storage was increased twofold after 18 h in cells depleted of Rab18 or its GEF, suggesting there is a link between Rab18 function and lipid droplets.

However, there was also increased association of ER sheets with lipid droplets in Rab18- or Rab18 GEF–depleted cells. One possibility is that this could facilitate lipid storage without requiring a direct role for Rab18 or its GEF complex.

Relationship of ER-shaping factors and human disease

A sobering feature of the proteins associated with ER network formation is their mutation in a spectrum of human neurological disorders (Blackstone, 2012). Atlastins, spastin, reticulon 2, REEP1, and REEP2 are all mutated in hereditary spastic paraplegia (Hazan et al., 1999; Park et al., 2010; Montenegro et al., 2012; Fink, 2013; Esteves et al., 2014), whereas Rab18 and the Rab3GAP1 and Rab3GAP2 subunits are mutated in Warburg Micro syndrome (Aligianis et al., 2005, 2006; Bem et al., 2011; Handley and Aligianis, 2012; Handley et al., 2013). In each case, these diseases are associated with progressive ascending spasticity. Other evidence supports the idea that Warburg Micro syndrome and hereditary spastic paraplegias (HSPs) should be considered as related disorders. A combination of mouse and human genetics has shown that the ER transmembrane protein TBC1D20 is mutated in Warburg Micro syndrome and the blind sterile mouse (Liegel et al., 2013). This is notable because TBC1D20 is a GAP for Rab1 and Rab2, and interacts with the reticulon family of proteins in the ER (Haas et al., 2007). TBC1D20 therefore provides a link between Warburg Micro syndrome and the reticulon family of ER-shaping proteins mutated in some hereditary spastic paraplegias. Other evidence linking HSPs and Warburg Micro syndrome is provided by the identification of Rab3GAP2 mutations in corticospinal motor neuron disease (Novarino et al., 2014), an autosomal-recessive HSP. This correlation between altered ER structure and neurological disorders is intriguing, and provides further support for the view that ER form and function are closely linked. As already mentioned, diverse cellular processes are associated with the ER, and explaining the dependencies on structural organization will be a complex task requiring the generation of specific experimental models to look at ER structure–function relationships in neuronal cells and during development.

Materials and methods

Reagents and antibodies

General laboratory chemicals were obtained from Sigma-Aldrich and Thermo Fisher Scientific. Duplexes for Rab18, Rab3GAP1, and Rab3GAP2 siRNA were obtained from Thermo Fisher Scientific and the sequences are listed in Table S1. A luciferase duplex was used as a control in all siRNA experiments. Commercially available antibodies were used to α-tubulin (mouse DM1A; Sigma-Aldrich), Myc-epitope (mouse clone 9E10; Sigma-Aldrich), FLAG-epitope (mouse monoclonal M2; Sigma-Aldrich), Rab7 (rabbit clone D95F2; Cell Signaling Technology), Rab10 (rabbit D36C4; Cell Signaling Technology), Rab18 (mouse 60057 and rabbit polyclonal; ProteinTech), Rab3GAP1 (rabbit 21663; ProteinTech), Rab3GAP2 (rabbit NBP1-84199; Novus Biologicals), GM130 (mouse clone 35; BD), β-COP (mouse G6160; Sigma-Aldrich), Sec31 (mouse clone 32; BD), TGN46 (sheep; AbD Serotec), LMAN1/ERGIC-53 (mouse 1A8; Novus Biologicals), calnexin (rabbit 10427; ProteinTech), ERp72 (rabbit clone D70D12; Cell Signaling Technology), PDI (rabbit clone C81H6; Cell Signaling Technology), GRP78/BiP (rabbit ab21685; Abcam), EEA1 (mouse clone 14; BD), LAMP1 (mouse clone H4A3; BD), NOGOA/Rtn4 (rabbit; AbD Serotec), and CLIMP-63 (mouse; Enzo Life Sciences). Affinity-purified sheep anti-GFP polyclonal was made previously by us. Secondary antibodies raised in donkey to mouse, rabbit, sheep/goat, and human conjugated to HRP, Alexa 488, -555, -568, and -647 were obtained from Molecular Probes and Jackson ImmunoResearch Laboratories, Inc.

Molecular biology and Rab protein expression

Human Rab GTPases were amplified using PCR from human testis, fetus, and liver cDNA and cloned into pFAT2 for bacterial expression or pGFP-C2 for eukaryotic expression of GFP-tagged Rabs (Fuchs et al., 2007; Yoshimura et al., 2010). Human Rab3GAP1 and Rab3GAP2 were amplified by PCR from human testis cDNA. Point mutations were introduced using the QuikChange method. Mammalian expression constructs were made using pcDNA4/TO and pcDNA5/FRT/TO vectors (Invitrogen). Mitochondrial targeted Rab3GAP was created in pcDNA5 by fusing the mitochondrial outer membrane targeting sequence of yeast Tom70p and three copies of the FLAG epitope sequence to the 5-prime end of the Rab3GAP1 or Rab3GAP2 cDNA. Rab proteins in pFAT2 were expressed in BL21 (DE3) pRIL at 18°C for 12–14 h. Cell pellets were disrupted in 20 ml IMAC20 (20 mM Tris-HCl, pH 8.0, 300 mM NaCl, 20 mM imidazole, and protease inhibitor cocktail; Roche) using an Emulsiflex C-5 system (Avestin, Inc.). Lysates were clarified by centrifugation at 16,000 rpm in a rotor (model JA-17; Beckman Coulter) for 30 min. To purify the tagged protein, 0.5 ml of nickel-charged NTA-agarose (QIAGEN) was added to the clarified lysate and rotated for 2 h. The agarose was washed three times with IMAC20 and the bound proteins eluted in IMAC200 (IMAC20 with 200 mM imidazole) collecting 1.5-ml fractions. All manipulations were performed on ice or in an 8°C cold room. Purified proteins were dialyzed against TBS (50 mM Tris-HCl, pH 7.4, and 150 mM NaCl) and then snap-frozen in liquid nitrogen for storage at −80°C. Protein concentration was measured using the Bradford assay.

Cell culture

Patient cell lines, HeLa, HEK293, and COS7 cells were cultured in DMEM containing 10% bovine calf serum (Invitrogen) at 37°C and 5% CO_2. For plasmid and siRNA transfection Mirus LT1 (Mirus Bio LLC) and Oligofectamine (Invitrogen), respectively, were used according to the manufacturer's instructions. For RNA interference experiments HeLa cells were plated at 18,000 cells per well and COS7 cells at 8,000 cells per well of a 6-well plate, respectively.

Purification of GEF complexes

FLAG- and Myc-tagged forms of Rab3GAP1 and Rab3GAP2 were transiently expressed in 8 × 15-cm dishes of 70% confluent HEK293T cells. For this purpose 800 µl OptiMEM (Invitrogen) was mixed with 24 µl Mirus LT1, and after 5 min 6 µg of each plasmid DNA was added. After 25 min this transfection mix was added to the cells. After 40 h of growth the cell pellet was lysed for 20 min on ice in 5 ml cell lysis buffer (50 mM Tris-HCl, pH7.4, 1 mM EDTA, 150 mM NaCl, 0.5% [vol/vol] Triton-X 100, and protease inhibitor cocktail). Cell extracts were split into 1-ml aliquots and clarified by centrifugation at 20,000 *g* in a microfuge (model 5417R; Eppendorf) for 20 min. The FLAG-tagged proteins were isolated from the clarified cell lysate using 100 µl anti-FLAG M2 affinity gel (Sigma-Aldrich) for 4 h at 4°C. The beads were washed ten times with 1 ml of cell lysis buffer, high salt buffer (50 mM Tris-HCl, pH 7.4, and 500 mM NaCl), and TBS, and then the proteins were eluted with 100 µl (200 µg/ml) FLAG-peptide in TBS containing 2 mM dithiothreitol. Eluted proteins were analyzed on 7.5–10% SDS-PAGE gels stained with Coomassie brilliant blue, and concentrations estimated by comparison to a series of bovine serum albumin standards in the range of 0.1 mg to 1 mg. The peak fractions were snap-frozen in liquid nitrogen for storage at −80°C without dialysis.

Nucleotide binding and Rab GEF screening

GEF assays were performed as described previously (Yoshimura et al., 2010). Nucleotide loading was performed as follows: 10 µg GST-tagged Rab was incubated in 50 mM Hepes-NaOH, pH 6.8, 0.1 mg/ml BSA, 125 µM EDTA, 10 µM Mg-GDP, and 5 µCi [^{3}H]-GDP (10 mCi/ml; 5,000 Ci/mmol) in a total volume of 200 µl for 20 min at 4°C. For standard GDP-releasing GEF assays, 100 µl of the loading reaction was mixed with 10 µl (10 mM) Mg-GTP, 10–100 nM GEF, or a buffer control, and adjusted with assay buffer to a final volume of 120 µl. The GEF reaction occurred for 20 min at 30°C. After this, 2.5 µl were taken for a specific activity measurement, and the remainder was split into two tubes, then incubated with 500 µl ice-cold assay buffer containing 1 mM $MgCl_2$ and 20 µl packed glutathione–Sepharose for 60 min at 4°C. After three washes with 500 µl ice-cold assay buffer the Sepharose was transferred to a vial containing

4 ml scintillation fluid and counted. The amount of nucleotide exchange was calculated in pmoles GDP-released. For GTP-binding assays the following modifications were made: only unlabeled GDP was used in the loading reaction; in the GEF reaction 0.5 µl (10 mM) GTP and 1 µCi [^{35}S]-GTPγS (10 mCi/ml; 5,000 Ci/mmol) were used. The amount of nucleotide exchange was calculated in pmoles GTP-bound.

Kinetic analysis of GEF activity

First, 10 nmol of hexahistidine-GST-Rab was loaded with 2′-(3′)-bis-*O*-(*N*-methylanthraniloyl)-GDP (Mant-GDP; Jena Bioscience) in 20 mM Hepes, pH 6.8, 1 mg/ml BSA, 20 mM EDTA, pH 8.0, and 40 mM Mant-GDP at 30°C for 30 min. After loading, 25 mmol $MgCl_2$ was added and the sample was exchanged into reaction buffer (20 mM Hepes, pH 6.8, 1 mg/ml BSA, 150 mM NaCl, and 1 mM $MgCl_2$) using Zeba spin columns (Thermo Fisher Scientific). Nucleotide exchange was measured using 1 nmol of the loaded Rab and the amount of GEF was specified in the figure legends in a final volume of 100 µl reaction buffer by monitoring the quenching of fluorescence after release of Mant-GDP using a Tristar LB 941 plate reader (Berthold Technologies) under control of MikroWin software. Samples were excited at 350 nm and emission monitored at 440 nm. GTP was added to a final concentration of 0.1 mM to start the exchange reaction at 30°C. Curve fitting and extraction of pseudo first-order rate constants (k_{obs}) was performed as described previously (Delprato et al., 2004; Delprato and Lambright, 2007). Because $k_{obs} = (k_{cat}/K_m)$ [GEF] + k_{basal}, where k_{basal} is the rate constant measured in the absence of GEF, catalytic efficiency (k_{cat}/K_m) can be obtained.

Rab GAP assays

For Rab-loading reactions, 10 µl of assay buffer, 73 µl H_2O, 10 µl (10 mM) EDTA, pH 8.0, 5 µl of 1 mM GTP, 2 µl γ-[^{32}P]GTP (10 mCi/ml; 5,000 Ci/mmol; ICN), and 100 pmol Rab protein were mixed on ice. GAP reactions were started by the addition of 0.5 pmol Rab3GAP1 mixed with 5.0 pmol Rab3GAP2 or buffer as specified in the figures. A 2.5-µl aliquot of the assay mix was scintillation counted to measure the specific activity in cpm/pmol GTP. Reactions were then incubated at 30°C for 60 min. The 5-µl aliquots were immediately added to 795 µl of ice-cold 5% (wt/vol) activated charcoal slurry in 50 mM NaH_2PO_4, left for 1 h on ice, and centrifuged at 16,100 *g* in a benchtop microfuge (model 5417R; Eppendorf) to pellet the charcoal. A 400-µl aliquot of the supernatant was scintillation counted, and the amount of GTP hydrolyzed was calculated from the specific activity of the reaction mixture.

MitoGEF assays

For MitoGEF assays, HeLa cells were seeded on no. 1.5 glass coverslips (Menzel-Gläser; Thermo Fisher Scientific) at a density of 30,000 cells per well on a 12-well plate, and then left for 30 h to adhere. The cells were transfected with 0.25 µg of mitochondrial-targeted Tom70-3xFLAG-Rab3GAP2, Myc-Rab3GAP1, and GFP-tagged Rab GTPases in combination using 1.5 µl Mirus LT1 in 50 µl OptiMEM. After 20 h the cells were processed for microscopy.

Membrane fractionations

For membrane fractionation the cells were washed from the dish in PBS containing 1 mM EDTA, then homogenized using 20 passes through an 18-gauge needle in 50 mM Hepes-NaOH, pH 7.4, and 200 mM sucrose. Unbroken cells were removed by centrifugation at 1,000 *g* for 10 min in a microfuge. A membrane pellet and cytosol were prepared from this post-nuclear supernatant by centrifugation at 100,000 *g* for 60 min in a rotor (model TLA-100; Beckman Coulter). Equivalent proportions of the membrane pellet and cytosol were analyzed by Western blotting.

Fixed-cell and live-cell microscopy

For fixed-cell imaging, cells were grown on no. 1.5 glass coverslips, washed twice with 2 ml of PBS, and fixed for 2 h in 2 ml PLP (2% [wt/vol] paraformaldehyde in 87.5 mM lysine, 87.5 mM sodium phosphate, pH 7.4, and 10 mM sodium periodate). Coverslips were washed three times in 2 ml (100 mM) sodium phosphate, pH 7.4, before permeabilization in 1 mg/ml BSA, 0.12 mg/ml saponin, and 100 mM sodium phosphate, pH 7.4, for 30 min. In all cases primary and secondary antibody staining was performed in PBS for 60 min at room temperature. Affinity-purified antibodies were used at 1 µg/ml; commercial antibodies were used as directed by the manufacturers. DAPI was added to the secondary antibody staining solution at 0.3 µg/ml. Coverslips were mounted in Mowiol 4-88 mounting medium (EMD Millipore). Fixed samples on glass slides were imaged using a 60×/1.35 NA oil immersion objective on an upright microscope (model BX61; Olympus) with filtersets for DAPI, GFP/Alexa 488, -555, -568, and -647 (Chroma Technology Corp.), a camera (CoolSNAP HQ^2; Roper Scientific), and MetaMorph 7.5 imaging software (Molecular Dynamics Inc.). Illumination was provided by a Lumen 200-Watt metal halide light source (Prior Scientific, Inc.). Image stacks of 12–35 planes with a spacing of 0.2–0.4 µm through the cell volume were taken. Image stacks were maximum intensity projected and then merged to create 24-bit RGB TIFF files in MetaMorph. Images in 24-bit RGB format were then cropped in Photoshop CS3 and placed into Illustrator CS3 (Adobe Systems Inc.) to produce the figures.

For live-cell imaging using spinning-disk confocal microscopy, cells were plated in 35-mm dishes with a 14-mm no. 1.5 coverglass window in the bottom (MatTek Corporation). For imaging, the dishes were placed in a 37°C and 5% CO_2 environment chamber (Tokai Hit) on the microscope stage. Imaging was performed at 37°C in 5% CO_2 using an inverted microscope (model IX81; Olympus) with a 60×/1.42 NA oil immersion objective coupled to an Ultraview Vox spinning-disk confocal system (PerkinElmer) fitted with an EM-CCD camera (model C9100-13; Hamamatsu Photonics). Exposure times were 50 ms using 6% laser power. Image stacks of six planes spaced 0.2 µm apart were taken at the time intervals shown in the figure for up to 1 h. A bright-field reference image was also taken to visualize cell shape. Maximum intensity projection of the fluorescent channels was performed in Volocity (PerkinElmer) to create 24-bit RGB TIFF files. Images in 24-bit RGB TIFF format were then placed into Adobe Illustrator CS3 to produce the figures.

Lipid storage assays

Oleate–BSA complexes were formed by incubating 2.1 mM fatty acid–free bovine serum albumin with 12.3 mM oleic acid in 100 mM Tris-HCl, pH 8.0, at 22°C for 5 h. Oleate–BSA stock solution was sterilized by passage through a 0.2-µm filter and stored at −20°C in small aliquots. To induce lipid droplet formation, cells were incubated with 400 µM oleate in DME containing 10% bovine calf serum for 18 h. For experiments where lipid droplet turnover was studied, cells were then washed three times in fresh growth medium and then grown for a further 12–36 h. The cells were then fixed with PLP and processed using the standard immunofluorescence protocol described already. Lipid droplets were detected with 1 µg/ml BODIPY 493/503 (4,4-difluoro-1,3,5,7,8-pentamethyl-4-bora-3a,4a-diaza-*s*-indacene; Molecular Probes) added to the secondary antibody-staining step.

Online supplemental material

Fig. S1 shows the biochemical analysis of Rab3GAP1 specificity and confirms depletion of the Rab18 and Rab3GAP complex using specific antibodies. Fig. S2 shows the effects of Rab18 and Rab3GAP depletion and additional ER and Golgi markers. Fig. S3 compares the localization of Rab18 and Rab10 to the ER in HeLa and COS7 cells. Figs. S4 and S5 show lipid storage dynamics in cells depleted of Rab18, Rab3GAP complex, or TBC1D20. Videos 1–5 show ER and Rab18 dynamics in control and Rab3GAP- and Rab18-depleted cells. Videos 6–8 show the rescue of ER tubular network dynamics by re-expressing mCherry-Rab18 in cells depleted of endogenous Rab18. Video 9 shows a comparison of lipid droplet and Rab18 dynamics on the ER. Table S1 contains details of the sequences used for RNA interference. Online supplemental material is available at http://www.jcb.org/cgi/content/full/jcb.201403026/DC1.

A Wellcome Senior Investigator Award (097769/Z/11/Z) to F.A. Barr supported this work. M.T. Handley and I. Aligianis were supported by the Newlife foundation for disabled children (07-08/12) and the MRC (RA1631 and RA1905).

The authors declare no competing financial interests.

Submitted: 7 March 2014
Accepted: 15 April 2014

References

Aligianis, I.A., C.A. Johnson, P. Gissen, D. Chen, D. Hampshire, K. Hoffmann, E.N. Maina, N.V. Morgan, L. Tee, J. Morton, et al. 2005. Mutations of the catalytic subunit of RAB3GAP cause Warburg Micro syndrome. *Nat. Genet.* 37:221–223. http://dx.doi.org/10.1038/ng1517

Aligianis, I.A., N.V. Morgan, M. Mione, C.A. Johnson, E. Rosser, R.C. Hennekam, G. Adams, R.C. Trembath, D.T. Pilz, N. Stoodley, et al. 2006. Mutation in Rab3 GTPase-activating protein (RAB3GAP) noncatalytic subunit in a kindred with Martsolf syndrome. *Am. J. Hum. Genet.* 78:702–707. http://dx.doi.org/10.1086/502681

Barr, F.A. 2013. Review series: Rab GTPases and membrane identity: causal or inconsequential? *J. Cell Biol.* 202:191–199. http://dx.doi.org/10.1083/jcb.201306010

Bem, D., S. Yoshimura, R. Nunes-Bastos, F.C. Bond, M.A. Kurian, F. Rahman, M.T. Handley, Y. Hadzhiev, I. Masood, A.A. Straatman-Iwanowska, et al. 2011. Loss-of-function mutations in RAB18 cause Warburg Micro syndrome. *Am. J. Hum. Genet.* 88:499–507. http://dx.doi.org/10.1016/j.ajhg.2011.03.012

Blackstone, C. 2012. Cellular pathways of hereditary spastic paraplegia. *Annu. Rev. Neurosci.* 35:25–47. http://dx.doi.org/10.1146/annurev-neuro-062111-150400

Blümer, J., J. Rey, L. Dehmelt, T. Mazel, Y.W. Wu, P. Bastiaens, R.S. Goody, and A. Itzen. 2013. RabGEFs are a major determinant for specific Rab membrane targeting. *J. Cell Biol.* 200:287–300. http://dx.doi.org/10.1083/jcb.201209113

Dejgaard, S.Y., A. Murshid, A. Erman, O. Kizilay, D. Verbich, R. Lodge, K. Dejgaard, T.B. Ly-Hartig, R. Pepperkok, J.C. Simpson, and J.F. Presley. 2008. Rab18 and Rab43 have key roles in ER-Golgi trafficking. *J. Cell Sci.* 121:2768–2781. http://dx.doi.org/10.1242/jcs.021808

Delprato, A., and D.G. Lambright. 2007. Structural basis for Rab GTPase activation by VPS9 domain exchange factors. *Nat. Struct. Mol. Biol.* 14:406–412. http://dx.doi.org/10.1038/nsmb1232

Delprato, A., E. Merithew, and D.G. Lambright. 2004. Structure, exchange determinants, and family-wide rab specificity of the tandem helical bundle and Vps9 domains of Rabex-5. *Cell*. 118:607–617. http://dx.doi.org/10.1016/j.cell.2004.08.009

Elias, M., A. Brighouse, C. Gabernet-Castello, M.C. Field, and J.B. Dacks. 2012. Sculpting the endomembrane system in deep time: high resolution phylogenetics of Rab GTPases. *J. Cell Sci.* 125:2500–2508. http://dx.doi.org/10.1242/jcs.101378

English, A.R., and G.K. Voeltz. 2013. Rab10 GTPase regulates ER dynamics and morphology. *Nat. Cell Biol.* 15:169–178. http://dx.doi.org/10.1038/ncb2647

Esteves, T., A. Durr, E. Mundwiller, J.L. Loureiro, M. Boutry, M.A. Gonzalez, J. Gauthier, K.H. El-Hachimi, C. Depienne, M.P. Muriel, et al. 2014. Loss of association of REEP2 with membranes leads to hereditary spastic paraplegia. *Am. J. Hum. Genet.* 94:268–277. http://dx.doi.org/10.1016/j.ajhg.2013.12.005

Fink, J.K. 2013. Hereditary spastic paraplegia: clinico-pathologic features and emerging molecular mechanisms. *Acta Neuropathol.* 126:307–328. http://dx.doi.org/10.1007/s00401-013-1115-8

Friedman, J.R., and G.K. Voeltz. 2011. The ER in 3D: a multifunctional dynamic membrane network. *Trends Cell Biol.* 21:709–717. http://dx.doi.org/10.1016/j.tcb.2011.07.004

Fuchs, E., A.K. Haas, R.A. Spooner, S. Yoshimura, J.M. Lord, and F.A. Barr. 2007. Specific Rab GTPase-activating proteins define the Shiga toxin and epidermal growth factor uptake pathways. *J. Cell Biol.* 177:1133–1143. http://dx.doi.org/10.1083/jcb.200612068

Fukui, K., T. Sasaki, K. Imazumi, Y. Matsuura, H. Nakanishi, and Y. Takai. 1997. Isolation and characterization of a GTPase activating protein specific for the Rab3 subfamily of small G proteins. *J. Biol. Chem.* 272:4655–4658. http://dx.doi.org/10.1074/jbc.272.8.4655

Gerondopoulos, A., L. Langemeyer, J.R. Liang, A. Linford, and F.A. Barr. 2012. BLOC-3 mutated in Hermansky-Pudlak syndrome is a Rab32/38 guanine nucleotide exchange factor. *Curr. Biol.* 22:2135–2139. http://dx.doi.org/10.1016/j.cub.2012.09.020

Gronemeyer, T., S. Wiese, S. Grinhagens, L. Schollenberger, A. Satyagraha, L.A. Huber, H.E. Meyer, B. Warscheid, and W.W. Just. 2013. Localization of Rab proteins to peroxisomes: a proteomics and immunofluorescence study. *FEBS Lett.* 587:328–338. http://dx.doi.org/10.1016/j.febslet.2012.12.025

Haas, A.K., S. Yoshimura, D.J. Stephens, C. Preisinger, E. Fuchs, and F.A. Barr. 2007. Analysis of GTPase-activating proteins: Rab1 and Rab43 are key Rabs required to maintain a functional Golgi complex in human cells. *J. Cell Sci.* 120:2997–3010. http://dx.doi.org/10.1242/jcs.014225

Handley, M.T., and I.A. Aligianis. 2012. RAB3GAP1, RAB3GAP2 and RAB18: disease genes in Micro and Martsolf syndromes. *Biochem. Soc. Trans.* 40:1394–1397. http://dx.doi.org/10.1042/BST20120169

Handley, M.T., D.J. Morris-Rosendahl, S. Brown, F. Macdonald, C. Hardy, D. Bem, S.M. Carpanini, G. Borck, L. Martorell, C. Izzi, et al. 2013. Mutation spectrum in RAB3GAP1, RAB3GAP2, and RAB18 and genotype-phenotype correlations in Warburg Micro syndrome and Martsolf syndrome. *Hum. Mutat.* 34:686–696. http://dx.doi.org/10.1002/humu.22296

Hazan, J., N. Fonknechten, D. Mavel, C. Paternotte, D. Samson, F. Artiguenave, C.S. Davoine, C. Cruaud, A. Dürr, P. Wincker, et al. 1999. Spastin, a new AAA protein, is altered in the most frequent form of autosomal dominant spastic paraplegia. *Nat. Genet.* 23:296–303. http://dx.doi.org/10.1038/15472

Hu, J., Y. Shibata, P.P. Zhu, C. Voss, N. Rismanchi, W.A. Prinz, T.A. Rapoport, and C. Blackstone. 2009. A class of dynamin-like GTPases involved in the generation of the tubular ER network. *Cell*. 138:549–561. http://dx.doi.org/10.1016/j.cell.2009.05.025

Klopfenstein, D.R., J. Klumperman, A. Lustig, R.A. Kammerer, V. Oorschot, and H.P. Hauri. 2001. Subdomain-specific localization of CLIMP-63 (p63) in the endoplasmic reticulum is mediated by its luminal alpha-helical segment. *J. Cell Biol.* 153:1287–1300. http://dx.doi.org/10.1083/jcb.153.6.1287

Klöpper, T.H., N. Kienle, D. Fasshauer, and S. Munro. 2012. Untangling the evolution of Rab G proteins: implications of a comprehensive genomic analysis. *BMC Biol.* 10:71. http://dx.doi.org/10.1186/1741-7007-10-71

Langemeyer, L., R. Nunes Bastos, Y. Cai, A. Itzen, K.M. Reinisch, and F.A. Barr. 2014. Diversity and plasticity in Rab GTPase nucleotide release mechanism has consequences for Rab activation and inactivation. *Elife*. 3:e01623. http://dx.doi.org/10.7554/eLife.01623

Lerner, D.W., D. McCoy, A.J. Isabella, A.P. Mahowald, G.F. Gerlach, T.A. Chaudhry, and S. Horne-Badovinac. 2013. A Rab10-dependent mechanism for polarized basement membrane secretion during organ morphogenesis. *Dev. Cell*. 24:159–168. http://dx.doi.org/10.1016/j.devcel.2012.12.005

Liegel, R.P., M.T. Handley, A. Ronchetti, S. Brown, L. Langemeyer, A. Linford, B. Chang, D.J. Morris-Rosendahl, S. Carpanini, R. Posmyk, et al. 2013. Loss-of-function mutations in TBC1D20 cause cataracts and male infertility in blind sterile mice and Warburg Micro syndrome in humans. *Am. J. Hum. Genet.* 93:1001–1014. http://dx.doi.org/10.1016/j.ajhg.2013.10.011

Lütcke, A., R.G. Parton, C. Murphy, V.M. Olkkonen, P. Dupree, A. Valencia, K. Simons, and M. Zerial. 1994. Cloning and subcellular localization of novel rab proteins reveals polarized and cell type-specific expression. *J. Cell Sci.* 107:3437–3448.

Martin, S., K. Driessen, S.J. Nixon, M. Zerial, and R.G. Parton. 2005. Regulated localization of Rab18 to lipid droplets: effects of lipolytic stimulation and inhibition of lipid droplet catabolism. *J. Biol. Chem.* 280:42325–42335. http://dx.doi.org/10.1074/jbc.M506651200

Montenegro, G., A.P. Rebelo, J. Connell, R. Allison, C. Babalini, M. D'Aloia, P. Montieri, R. Schüle, H. Ishiura, J. Price, et al. 2012. Mutations in the ER-shaping protein reticulon 2 cause the axon-degenerative disorder hereditary spastic paraplegia type 12. *J. Clin. Invest.* 122:538–544. http://dx.doi.org/10.1172/JCI60560

Nagano, F., T. Sasaki, K. Fukui, T. Asakura, K. Imazumi, and Y. Takai. 1998. Molecular cloning and characterization of the noncatalytic subunit of the Rab3 subfamily-specific GTPase-activating protein. *J. Biol. Chem.* 273:24781–24785. http://dx.doi.org/10.1074/jbc.273.38.24781

Novarino, G., A.G. Fenstermaker, M.S. Zaki, M. Hofree, J.L. Silhavy, A.D. Heiberg, M. Abdellateef, B. Rosti, E. Scott, L. Mansour, et al. 2014. Exome sequencing links corticospinal motor neuron disease to common neurodegenerative disorders. *Science*. 343:506–511. http://dx.doi.org/10.1126/science.1247363

Orso, G., D. Pendin, S. Liu, J. Tosetto, T.J. Moss, J.E. Faust, M. Micaroni, A. Egorova, A. Martinuzzi, J.A. McNew, and A. Daga. 2009. Homotypic fusion of ER membranes requires the dynamin-like GTPase atlastin. *Nature*. 460:978–983. http://dx.doi.org/10.1038/nature08280

Ozeki, S., J. Cheng, K. Tauchi-Sato, N. Hatano, H. Taniguchi, and T. Fujimoto. 2005. Rab18 localizes to lipid droplets and induces their close apposition to the endoplasmic reticulum-derived membrane. *J. Cell Sci.* 118:2601–2611. http://dx.doi.org/10.1242/jcs.02401

Park, S.H., P.P. Zhu, R.L. Parker, and C. Blackstone. 2010. Hereditary spastic paraplegia proteins REEP1, spastin, and atlastin-1 coordinate microtubule interactions with the tubular ER network. *J. Clin. Invest.* 120:1097–1110. http://dx.doi.org/10.1172/JCI40979

Pfeffer, S.R. 2013. Rab GTPase regulation of membrane identity. *Curr. Opin. Cell Biol.* 25:414–419. http://dx.doi.org/10.1016/j.ceb.2013.04.002

Rowland, A.A., and G.K. Voeltz. 2012. Endoplasmic reticulum-mitochondria contacts: function of the junction. *Nat. Rev. Mol. Cell Biol.* 13:607–625. http://dx.doi.org/10.1038/nrm3440

Sakane, A., S. Manabe, H. Ishizaki, M. Tanaka-Okamoto, E. Kiyokage, K. Toida, T. Yoshida, J. Miyoshi, H. Kamiya, Y. Takai, and T. Sasaki. 2006. Rab3 GTPase-activating protein regulates synaptic transmission and plasticity through the inactivation of Rab3. *Proc. Natl. Acad. Sci. USA*. 103:10029–10034. http://dx.doi.org/10.1073/pnas.0600304103

Salloum, S., H. Wang, C. Ferguson, R.G. Parton, and A.W. Tai. 2013. Rab18 binds to hepatitis C virus NS5A and promotes interaction between sites of viral replication and lipid droplets. *PLoS Pathog.* 9:e1003513. http://dx.doi.org/10.1371/journal.ppat.1003513

Shibata, Y., C. Voss, J.M. Rist, J. Hu, T.A. Rapoport, W.A. Prinz, and G.K. Voeltz. 2008. The reticulon and DP1/Yop1p proteins form immobile oligomers in the tubular endoplasmic reticulum. *J. Biol. Chem.* 283:18892–18904. http://dx.doi.org/10.1074/jbc.M800986200

Shibata, Y., T. Shemesh, W.A. Prinz, A.F. Palazzo, M.M. Kozlov, and T.A. Rapoport. 2010. Mechanisms determining the morphology of the peripheral ER. *Cell*. 143:774–788. http://dx.doi.org/10.1016/j.cell.2010.11.007

Vazquez-Martinez, R., D. Cruz-Garcia, M. Duran-Prado, J.R. Peinado, J.P. Castaño, and M.M. Malagon. 2007. Rab18 inhibits secretory activity in neuroendocrine cells by interacting with secretory granules. *Traffic*. 8:867–882. http://dx.doi.org/10.1111/j.1600-0854.2007.00570.x

Voeltz, G.K., and W.A. Prinz. 2007. Sheets, ribbons and tubules - how organelles get their shape. *Nat. Rev. Mol. Cell Biol.* 8:258–264. http://dx.doi.org/10.1038/nrm2119

Voeltz, G.K., W.A. Prinz, Y. Shibata, J.M. Rist, and T.A. Rapoport. 2006. A class of membrane proteins shaping the tubular endoplasmic reticulum. *Cell*. 124:573–586. http://dx.doi.org/10.1016/j.cell.2005.11.047

Wendler, F., A.K. Gillingham, R. Sinka, C. Rosa-Ferreira, D.E. Gordon, X. Franch-Marro, A.A. Peden, J.P. Vincent, and S. Munro. 2010. A genome-wide RNA interference screen identifies two novel components of the metazoan secretory pathway. *EMBO J.* 29:304–314. http://dx.doi.org/10.1038/emboj.2009.350

Wu, X., M.J. Bradley, Y. Cai, D. Kümmel, E.M. De La Cruz, F.A. Barr, and K.M. Reinisch. 2011. Insights regarding guanine nucleotide exchange from the structure of a DENN-domain protein complexed with its Rab GTPase substrate. *Proc. Natl. Acad. Sci. USA*. 108:18672–18677. http://dx.doi.org/10.1073/pnas.1110415108

Yoshimura, S., A. Gerondopoulos, A. Linford, D.J. Rigden, and F.A. Barr. 2010. Family-wide characterization of the DENN domain Rab GDP-GTP exchange factors. *J. Cell Biol.* 191:367–381. http://dx.doi.org/10.1083/jcb.201008051